Novel concepts of vacuum microelectronic microwave devices with field emitter cathode arrays

A. G. Rozhnev, N. M. Ryskin, D. V. Sokolov, and D. I. Trubetskov
Saratov State University, Saratov, Russia

S. T. Han, J. I. Kim, and G. S. Park
School of Physics, Seoul National University, Seoul, Korea

(Received 20 February 2002; accepted 6 June 2002)

Field emitter arrays (FEA) are promising electron sources for vacuum microelectronic microwave amplifiers and oscillators. In this paper, microelectronic analogs of ''classic'' microwave devices are considered. Traveling wave klystrons, klystrodes and cross-field amplifiers with FEA are described. Basic output parameters (gain, efficiency, etc.) of these devices are calculated. A model of a self-excited vacuum microtriode oscillator is developed. The oscillator is studied numerically, as well as by experimental investigation of the circuit analog model. Chaotic generation in the oscillator under external harmonic driving is analyzed. The rf interaction with the electron beam modulated by the field emission in a twystrode is investigated using a particle-in-cell code and a one-dimensional nonlinear code. © *2002 American Institute of Physics.*
[DOI: 10.1063/1.1497684]

I. INTRODUCTION

The development of various types of field emitter arrays (FEA) promised the creation of miniature vacuum amplifiers and oscillators in the microwave and millimeter wave bands. The main advantages of FEA are their high current density and transconductivity, and short electron transit time, in comparison with gridded thermionic cathodes. It was expected that the application of FEA would increase the operating frequency of emission-gated devices.[1–3] In addition, it was expected that such devices would possess temperature and radiation stability superior to solid-state devices. However, it has transpired that the existing parameters of FEA are insufficient for application in vacuum microtriodes, as well as in more complicated schemes, such as distributed amplifiers. The main shortcomings include:[1–4]

(1) The losses in thin conductive films at microwave frequencies are much higher than those in conventional triodes;
(2) in the distributed amplifiers, attenuation of the amplitude of the modulating field along the input line due to interaction with emitted electrons (electron damping) is essential;[4]
(3) the high input capacitance restricts the operating frequency of the field emission triode so that it is lower than that in similar solid-state devices.

The indicated circumstances have resulted in a search to find new schematics for amplifiers and oscillators with FEA, turning to ''classic'' vacuum microwave devices. In this paper, we consider several devices that seem to be promising. The microelectronic analogs of traveling wave klystrons (Sec. II), klystrodes (Sec. III) and cross-field amplifiers (Sec. IV) are described. In Sec. V the vacuum microtriode oscillator is analyzed. Driven by an external harmonic voltage, this oscillator can demonstrate complex oscillatory regimes, including quasiperiodic and chaotic. Thus, it has potential for the application in modern systems of information transmission and processing using chaos (e.g., see Ref. 5). In Sec. VI, using an electron beam modulated by field emission in twystrodes, as the microelectronic analogs of helix traveling wave tube (TWT), is investigated by numerical simulation. Note that klystrodes and twystrodes with FEA are currently under active investigation by a number of research teams.[6–9]

II. TRAVELING WAVE KLYSTRON WITH FIELD EMISSION CATHODE ARRAY

The traveling wave klystron (TWK) suggested by R. Kompfner in 1947 is a conventional klystron amplifier in which the input and output cavities are replaced by the waveguides and the electron gun is replaced either by the cathode extended along the waveguide, or by the set of guns (multibeam TWK). The microelectronic modification of the TWK[4] utilizes the microstrip transmission lines as the waveguide structures and FEA as the distributed cathode [Fig. 1(a)]. The device is quite similar to the distributed amplifier, except for the drift space. Due to velocity modulation in the input line, additional electron bunching occurs in the drift space, which provides gain enhancement.

Numerical simulation of the electron bunching in a drift space can be performed with the same Lagrange particle method that is widely used in the theory of vacuum microwave devices (klystrons, TWT, etc.) One can find a detailed description of the numerical technique in Ref. 10. The emitting surface extended along the y axis is divided into partial beams. Initial phases of electrons in each beam are chosen so that the emission current I satisfies the Fowler–Nordheim law[1–4]

$$I = aV^2 \exp(-b/V), \tag{1}$$

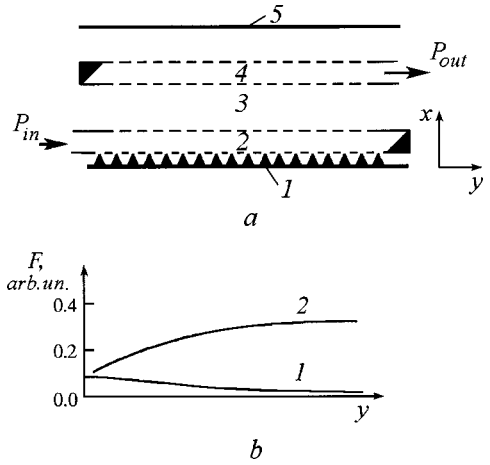

FIG. 1. (a) Schematic of the traveling wave klystron with FEA: 1—FEA, 2—input microstrip line, 3—drift space, 4—output microstrip line, 5—anode. (b) Field distributions in the input (1) and output (2) lines.

where $V=V_b+V_{\mathrm{hf}}(t,y)$, V_b is the constant bias voltage, $V_{\mathrm{hf}}(t,y)$ is the high-frequency voltage in the input waveguide, and a and b are constants which depend on emitter shape and material. At $y=0$ the input line is excited by a monochromatic signal of constant amplitude. In the input line the interaction with the emitted electrons should be taken into account. This interaction causes attenuation of the high-frequency voltage along the input line [Fig. 1(b)]. As a result, the high-frequency current that excites the output line after the drift space decreases, and quick saturation of field in the output line occurs.

The efficiency of the device may be improved by adding an intermediate microstrip line [Fig. 2(a)], similar to the conventional TWK.[4,11] Because the field in this line must provide additional bunching, its impedance must have inductive character, i.e., the phase of the voltage must outstrip that of the current. This effect can be achieved by, for example, bending the end of the line [Fig. 2(a)]. Electron bunches that enter the bent section receive additional velocity modulation due to phase delay from the field. This results in improved bunching in the drift space after the second line [Fig. 2(b)]. The voltage in the output line should be less than the beam accelerating voltage to forbid the electron reverse, so the wave impedance of the output line should be reduced near the end (for example, by narrowing the line). Numerical calculation reveals that for such a device, a 30% efficiency and 23 dB gain could be obtained in the millimeter band. The bandwidth of the amplifier is about 10%–20% (similar to conventional TWK) depending on the dispersion of waveguide structures.

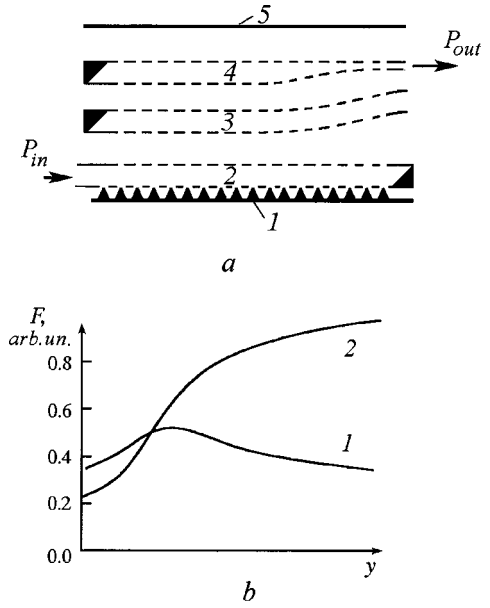

FIG. 2. (a) Schematic of the traveling wave klystron with the intermediate microstrip line (3). Other notations are the same as in Fig. 1(a). (b) Field distributions in the intermediate (1) and output (2) lines.

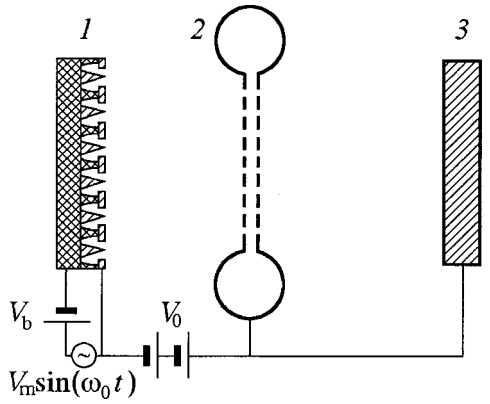

FIG. 3. Schematic of the klystrode with FEA: 1—FEA, 2—output cavity, 3—collector.

III. KLYSTRODE WITH FIELD EMISSION CATHODE ARRAY

One of the most promising emission-gated devices with gridded thermionic cathodes is a klystrode—a high-power UHF amplifier, combining the operating principles of the tetrode and klystron.[2,12–14] Application of the FEA to the klystrode attracts considerable interest because it is expected to increase the operating frequency, to at least 10 GHz.[6,7] The schematic of the klystrode with FEA is presented in Fig. 3. Note that this device is quite similar to the femitron,[15] but the application of FEA helps to increase the gain and to reduce the operating voltage.

Because in the klystrode the electron beam entering the drift space has no initial velocity modulation, it is to be expected that no electron overtaking will occur; so it is possible to use Euler variables for the numerical simulation fluid model of the beam instead of Lagrange particles. This approach, developed in Refs. 16–18, avoids the evaluation of initial phases of the electrons corresponding to the initial emission modulation. The beam is assumed to be strongly magnetized, so that the electron fluid velocity v has only an axial component. Under this assumption the equations of one-dimensional (1D) fluid model are

$$\frac{\partial v}{\partial t}+v\frac{\partial v}{\partial x}=-\frac{e}{m}(E+E_{\mathrm{sc}}),$$

$$\frac{\partial \rho}{\partial t}+\frac{\partial(\rho v)}{\partial x}=0, \tag{2}$$

where ρ is the electron charge density, and e and m are the electron charge and mass, respectively. To determine the space-charge field E_{sc} we use a well-known assumption that space-charge forces between two cross-sections of the beam decrease exponentially with the distance[10]

$$E_{sc}(x)=\frac{k_\perp}{4\pi\varepsilon_0}\int(\rho(x')-\rho_0)\exp[-k_\perp|x-x'|]\times\mathrm{sgn}(x-x')dx'. \tag{3}$$

Here ρ_0 is the neutralizing ion density, which is assumed to equal to the average electron density, and $k_\perp$ is the constant parameter depending on beam configuration. For example, for a cylindrical beam moving in a perfectly conducting drift tube, $k_\perp \approx 2/r_b$, where r_b is the beam radius.[10]

The axial component of the high-frequency electric field in the output gap is expressed as

$$E(x,t)=\mathrm{Re}[C_s(t)E_s(x)\exp(i\omega_s t)], \tag{4}$$

where ω_s is the resonant frequency. For the numerical simulation we use the simplest rectangular approximation of $E_s(x)$

$$E_s(x)=\begin{cases}0 & \text{if } x<x_1 \text{ or } x>x_2\\ V_0/d & \text{if } x_1\leqslant x\leqslant x_2\end{cases}, \tag{5}$$

where V_0 is the beam accelerating voltage, x_1 and x_2 are the positions of the beginning and the end of the gap, respectively, and $d=x_2-x_1$. Results for nonrectangular $E_s(x)$ were presented in Ref. 18. The complex amplitude $C_s(t)$ obeys the following equation:

$$\frac{dC_s}{dt}=-\frac{\omega_s C_s}{2Q_L}-\frac{\omega_s K}{2\pi V_0^2}\int_{x_1}^{x_2}\left[\int_0^{2\pi} I(x,t)E_s(x)\times\exp(-\omega_s t)d\omega_s t\right]dx, \tag{6}$$

where Q_L is the loaded quality of the cavity, and K is the cavity wave impedance.

We assume that the beam is injected in the drift tube at $x=0$ with constant velocity $v_0=\sqrt{2eV_0/m}$ and with the initial current modulation that satisfies the Fowler–Nordheim law (1) with $V=V_b+V_{hf}\sin(\omega_0 t)$. Note that basic equations (2), (3), (6) are fully nonstationary and are suitable for the simulation of nonharmonic signal amplification.

For efficient operation of the device, it is essential to obtain a well-bunched electron beam. Figure 4(a) demonstrates a plot of the first four current harmonics versus normalized signal amplitude $V'=V_{hf}/V_b$ for $b'=b/V_b=10.0$. Note that values of b', experimentally measured in Ref. 19, lie within the limits $5.0<b'<15.0$. Assuming that amplitude of the gap voltage is close to V_0 one can obtain a simple estimation of the efficiency as $I_1/2I_0$ for the amplifier and $I_n/2I_0$ for the multiplier (I_0 is the average beam current). Figure 4(a) shows that the klystrode with FEA is expected to be a highly efficient device.

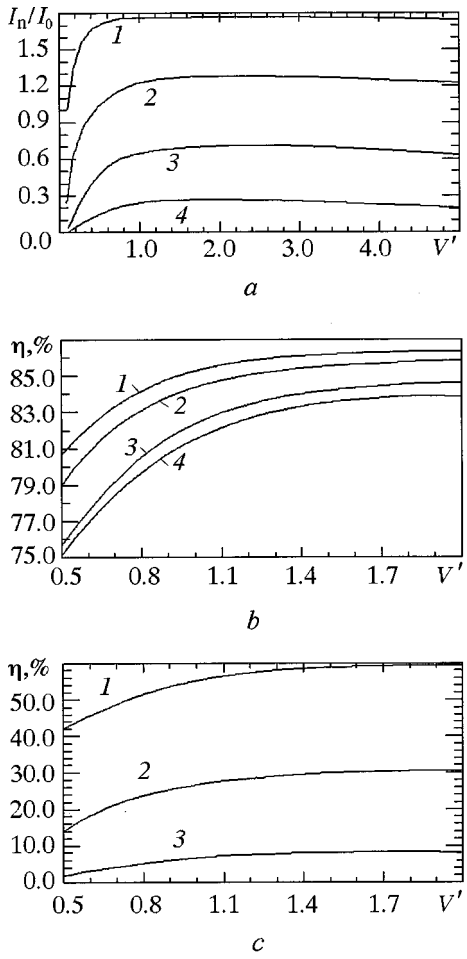

FIG. 4. (a) First four current harmonics I_n/I_0 versus normalized high-frequency voltage V' calculated according to the Fowler–Nordheim law for $b'=10.0$. (b) Efficiency η of the klystrode amplifier with FEA: 1—$b'=12.0$; 2—$b'=10.0$; 3—$b'=8.0$; 4—$b'=8.0$, space-charge effects are taken into account. (c) Efficiency η of the klystrode frequency multiplier for $b'=10.0$: 1—$n=2$; 2—$n=3$; 3—$n=4$.

For the numerical solution we have chosen $\phi_0=\pi/4$ and $\phi_1=\pi/2$, where $\phi_0=\omega_0 d/v_0$ is the electron transit angle in the cavity gap $\phi_1=\omega_0 x_1/v_0$. These values are typical for the klystrodes described in Refs. 12–14. Figure 4(b) shows efficiency η versus V' for different values of b' for the amplifier driven at resonant frequency ($\omega_0=\omega_s$). Figure 4(c) presents a similar plot for a frequency multiplier ($b'=10.0$). Our calculations reveal that space-charge effects are very weak and can usually be neglected. For each curve in Figs. 4(b) and 4(c) we have evaluated the optimal value of the cavity wave impedance K when the gap voltage is equal to V_0/M, where $M=\sin(\phi_0/2)/(\phi_0/2)$ (see Ref. 18). These results agree well with estimations made from Fig. 4(a), but the efficiency is somewhat lower, due to the interaction of the bunch with the field in the output gap.

The bandwidth of the device is determined by the bandwidth of the cavity. To increase the bandwidth one should apply the traveling-wave output structure instead of the narrow-band cavity.[6,7,9]

Numerical results reveal that the klystrode with FEA is an attractive, high-efficiency microwave device. Peak effi-

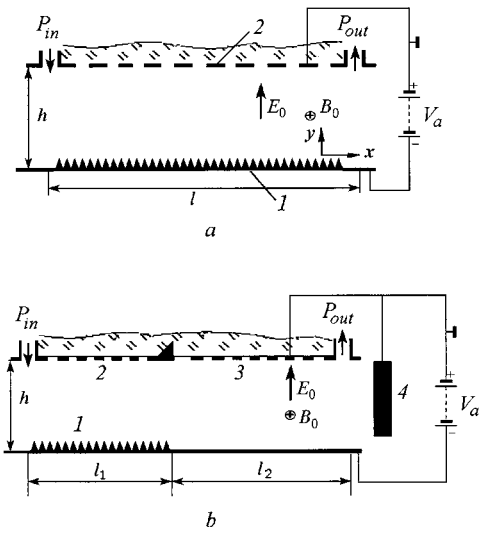

FIG. 5. (a)—Schematic drawing of the single-stage cross-field amplifier with FEA: 1—FEA; 2—slow-wave structure. (b)—Schematic drawing of the two-stage cross-field amplifier with FEA: 1—FEA; 2—input slow-wave structure; 3—output slow-wave structure; 4—collector.

ciencies can be up to 70%–80% for the amplifier and about 50% for the second harmonic multiplier. However, for such extremely high efficiencies, high-frequency voltage amplitude must be comparable with the bias voltage, and that will result in the reducing of gain and lifetime. Moderate modulation depth ($V' \sim 0.2$) that guarantees sufficiently good bunching and 60% efficiency seems to be preferable.

IV. MICROELECTRONIC CROSS-FIELD AMPLIFIERS WITH FEA

Microelectronic modifications of cross-field amplifiers (CFA) seem to be well suited to employing FEA.[4,20,21] The typical schematic for a device with crossed electrostatic E_0 and magnetostatic B_0 fields is presented on Fig. 5(a). In the upper plane, a slow-wave structure is placed, and on the lower plane an extended field emission cathode is arranged. Electrons emitted during the accelerating phase of the electromagnetic wave fall on the cathode surface, where they are absorbed. Electrons emitted during the decelerating phase rise to the slow wave structure, transferring their energy to the wave. The main advantages of the CFA are the following:

(1) No controlling grid is required, so the high grid-cathode capacitance does not restrict the operating frequency;
(2) it is possible to use disordered emitting surfaces (such as diamond-like carbon films, carbon nanotube films, etc) instead of uniform regular arrays;
(3) no electron focusing system is required;
(4) cross-field devices are usually characterized by high efficiency and high power output,[22] so one can expect their microelectronic analogs to have the same properties.

A number of special features of the microelectronic modification of the CFA must be noted.[4,20,21] In conventional devices the cyclotron radius $R = v_0/\omega_c$ ($\omega_c = eB_0/m$ is the cyclotron frequency, $v_0 = E_0/B_0$ is the static drift velocity) is usually much less than the distance from cathode to anode, $h: r = R/h \ll 1$; so the cyclotron rotation does not have a strong effect on the beam–wave interaction process. In the microelectronic design h is so small that electrons can fall on the anode during the first period of the cyclotron rotation and no interaction occurs. Assuming that the phase velocity of electromagnetic wave v_{ph} is equal to v_0, the following expressions for minimal values of B_0 and anode voltage $V_a = E_0 h$ could be obtained[4,20,21]

$$r = \frac{0.036f}{B_0 Y_h}, \quad V_a = \frac{5.11 \times 10^5}{rn^2}, \tag{7}$$

where f is frequency in GHz, $Y_h = \beta h$ is normalized cathode to anode distance, $\beta = 2\pi f n/c$, $n = c/v_{ph}$ is a delay factor, and c is the speed of light. In (7) B_0 is expressed in T, and V_a in kV. Limiting values of B_0 and V_a corresponding to $r = 0.5$ and $y = 4$ are listed in Tables I and II. From Table I it follows that in frequency range 50–200 GHz the desired values of the magnetic field may readily be attained. Table II shows that for $V_a < 1$ kV the delay factor should be more than 30, much higher than that required for conventional microwave devices. Fortunately, for microelectronic slow wave structures, values of n are approximately 20–80, typically due to the presence of a dielectric substrate.[23]

The motion of electrons in the CFA is governed by the following equations:[4]

$$\begin{aligned} \frac{dv_x}{d\tau} &= v_y - F_x, \\ \frac{dv_y}{d\tau} &= -v_x - F_y + \frac{1}{D}, \\ \frac{dX}{d\tau} &= \frac{\omega D}{\omega_c} v_x, \\ \frac{dY}{d\tau} &= \frac{\omega D}{\omega_c} v_y. \end{aligned} \tag{8}$$

TABLE I. Limiting values of magnetic field for different operating frequencies for cross-field amplifier with FEA.

Operating frequency f (GHz)	Magnetic field B_0 (T)
10	0.18
50	0.9
100	1.8
200	3.6
400	7.2

TABLE II. Limiting values of anode voltage for different delay factors for cross-field amplifier with FEA.

Delay factor n	Anode voltage V_a (kV)
10	10.2
20	2.55
30	1.23
50	0.41

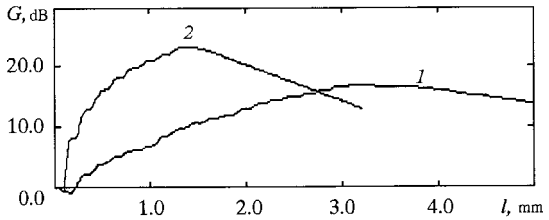

FIG. 6. Gain versus system length for the single-stage (1) and two-stage (2) cross-field amplifiers with FEA.

Here $\tau=\omega_c t$ is normalized time, $X=\beta x$ and $Y=\beta y$ are normalized coordinates, $v_x=(1/v_0D)(dx/dt)$ and $v_y=(1/v_0D)(dy/dt)$ are normalized components of velocity, $D=\sqrt{KJ_0/E_0}$ is a dimensionless interaction parameter, where K—coupling impedance and J_0—linear current density. Normalized components of the rf field, $F_{x,y}=E_{x,y}/(E_0D)$, can be expressed in the following form:[22]

$$F_x=(\sinh Y/\cosh Y_h)\mathrm{Re}[Fe^{-i(X-\tau)}],$$
$$F_y=(\cosh Y/\cosh Y_h)\mathrm{Re}[Fe^{-i(X-\tau)}]. \quad (9)$$

The complex amplitude F of the rf field can be found from the equation

$$\frac{dF}{dX}+irF=\frac{1}{2\pi q}\int_0^X\int_0^{2x}\frac{\sinh Y}{\sinh Y_h}e^{-i(X+\tau)}dX_0dX. \quad (10)$$

Here $r=(\Gamma-\beta)/\beta D$, Γ is the complex propagation constant in the cold slow-wave structure, q is the total length of the slow-wave structure, X_0 is initial phase of electron. We take the initial phases to be distributed uniformly over the wavelength.

In the simple CFA scheme [Fig. 5(a)] the emission current at the beginning of the cathode is small, so the microwave field excited by the current increases slowly along the x axis. Therefore, the length of the slow wave structure must be very large ($\approx 10\lambda$ where $\lambda=v_0/f$ is the delayed wavelength). On the other hand, long structures are undesirable because of high losses. To overcome this drawback a two-stage configuration was suggested[20,21] [Fig. 5(b)]. The field-emission cathode is placed only in the short input section, which serves to produce electron bunches. These bunches induce a microwave field in the output section, which serves to extract the energy from the beam.

Results of the numerical simulation of Eqs. (8)–(10) are presented in Figs. 6 and 7. The simulation algorithm[4,21] is quite similar to that of conventional cross-field tubes.[10] so we do not describe it in detail. Figure 6 demonstrates an example of a gain versus system length plot for single-stage and two-stage devices. It is evident that in the second case gain increment is much lighter and saturation length is much shorter. As a result, the system length can be reduced approximately 2.5 times, while the maximal gain increases by 7 dB. Figure 7 shows the maximal gain $G_{\max}$ versus linear current density J_0 for different values of loss parameter in the slow wave structure L. Note that even for high losses and moderate current densities it was possible to obtain sufficiently large gain.

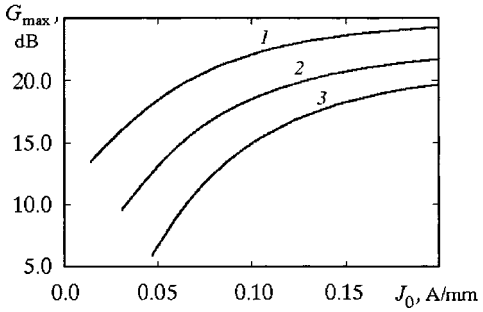

FIG. 7. Maximal gain $G_{\max}$ versus linear current density J_0 for different values of losses in the slow wave structure for the two-stage CFA: 1—$L=3$ dB/mm; 2—$L=6$ dB/mm; 3—$L=8$ dB/mm.

V. CHAOTIC GENERATION IN VACUUM MICROTRIODE OSCILLATOR

The application of concepts of nonlinear science such as solitons, chaos and patterns in microwave electronics is a subject of much current interest.[24] For example, for modern systems of information transmission and processing using chaos (for the review see Ref. 5), a chaotic oscillator based on a field-emission vacuum microtriode operating at microwave frequencies seems to have great potential. A schematic drawing of a self-excited oscillator with field-emission microtriode[24,25] is presented in Fig. 8(a). The device is quite similar to a conventional Van der Pol triode oscillator, but a nonlinear resistor R is included in the LC-circuit to prevent emitter breakdown. Nonlinear current-voltage characteristic of the resistor $I(V)$ is assumed to be exponential:

$$I=I_0[\exp(V/V_0)-1]. \quad (11)$$

Note that the ideal current-voltage characteristic of a semiconductor diode has the form (11) where $V_0=kT/e$ is the thermal potential.

The dynamics of the oscillator can be described by the following dimensionless equation:[4,24,25]

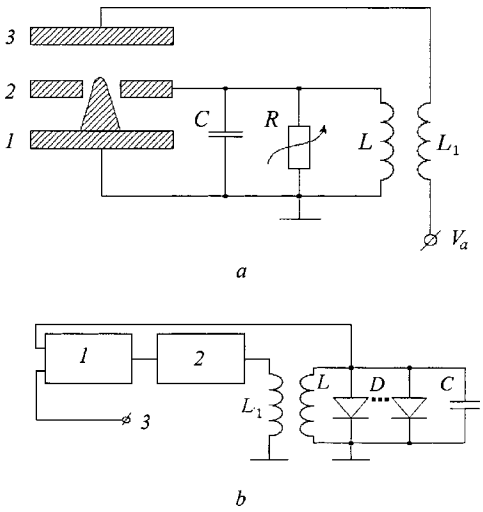

FIG. 8. (a)—Schematic drawing of a self-excited oscillator with field-emission microtriode: 1—emitter; 2—gate; 3—anode; (b)—Circuit analog model: 1—linear amplifier; 2—nonlinear amplifier; 3—external harmonic drive.

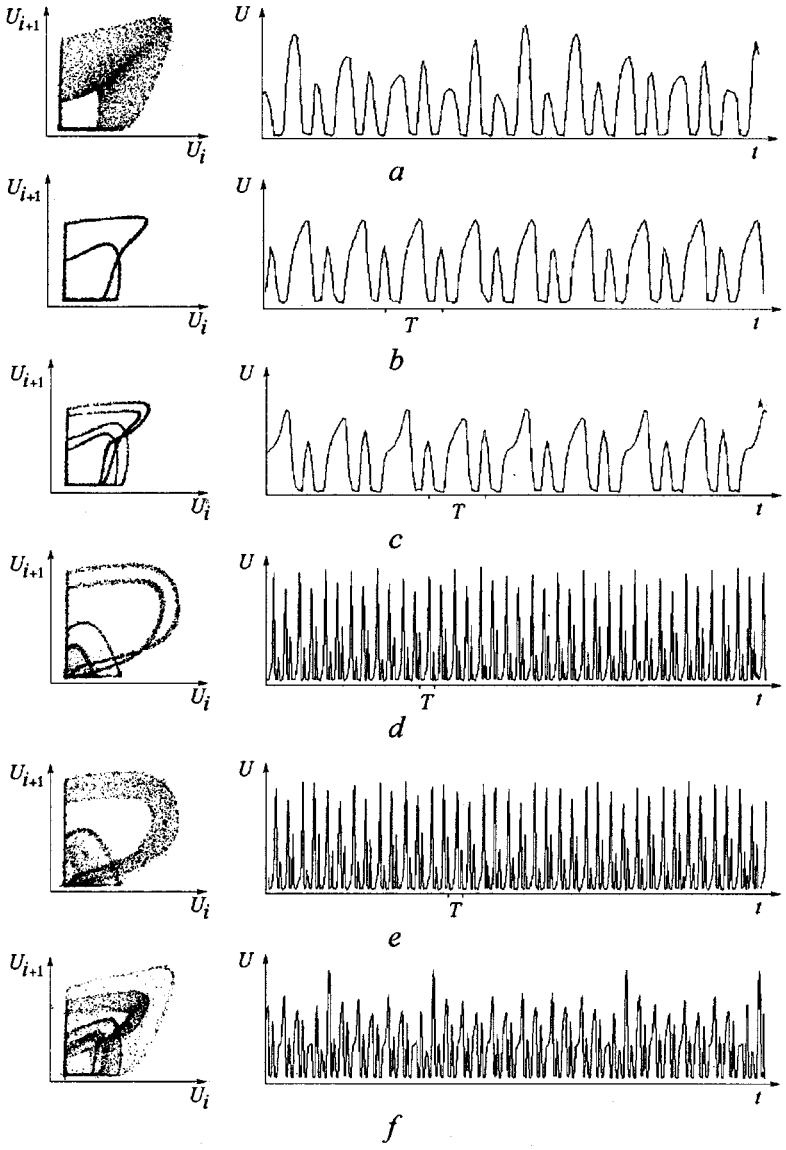

FIG. 9. Experimental voltage wave forms and phase portrait projections for an analog model of the vacuum microtriode oscillator: (a)—quasiperiodic oscillations; (b)—1:2 resonant cycle; (c)—doubled resonant cycle; (d) and (e)—chaotic oscillations; (f)—intermittency.

$$\frac{d^2U}{dt^2}+\left[g_0\exp(\kappa U)-\mu(2U+2\sigma+1)\times\exp\left(-\frac{1}{U+\sigma}\right)\right]\frac{dU}{dt}+U=\begin{cases}0, & \text{autonomous oscillator}\\ F\sin pt, & \text{oscillator driven by external harmonic signal}\end{cases}. \quad (12)$$

Here, U is the normalized grid voltage, g_0 and κ are resistor parameters, μ is the coupling coefficient, σ is the parameter of the microtriode current-voltage characteristic, F and p are amplitude and frequency of external driving, respectively, and t is the normalized time. All quantities in Eq. (9) are dimensionless.

Nonlinear dynamics of the vacuum microtriode oscillator was studied by numerical simulation, as well as by experimental investigation of a circuit analog model.[24,25] The latter [Fig. 8(b)] includes the LC-circuit with nonlinear resistive elements (diodes D) and the nonlinear amplifier 2 with exponential characteristic. The linear amplifier 1 serves to apply the external harmonic driving. The nonlinearity parameter σ is tuned by varying the gain of the linear amplifier, while the dissipation is tuned by changing the number of diodes.

In autonomous mode, when no external driving is applied, the oscillator (12) demonstrates either soft or hard excitation, depending on the control parameters. Finally, periodic nonlinear self-oscillations establish themselves, corresponding to a limit cycle on the phase plane.

Both numerical and experimental studies of the oscillator driven by the harmonic signal reveal a variety of possible dynamic regimes including periodic, quasiperiodic and chaotic oscillations. This is illustrated by Fig. 9, where the examples of experimental voltage wave forms and phase portrait projections $U_{j+1}=f(U_j)$ ($U_j=U(t_j)$, $t_{j+1}=t_j+T$, T is the period of driving signal) are presented. Quasiperiodic oscillations [Fig. 9(a)] have two basic frequencies that are in irrational relation. In the phase space, the attractors are 2D tori. Periodic oscillations correspond to synchronization re-

gimes when resonant cycles appear on the tori. Figures 9(b) and 9(c) demonstrate 1:2 and 1:4 resonance cycles which form as a result of a period-doubling bifurcation. In Figs. 9(d) and 9(e) two different types of chaotic oscillations are presented. Finally, Fig. 9(f) shows the regime of intermittency where almost regular oscillations are interrupted by nonperiodic bursts. The results of numerical and experimental modeling are in a qualitative agreement.

VI. ELECTRON BEAM MODULATED BY FIELD EMISSION IN TWYSTRODE

It is expected that the electron beam modulated at microwave frequencies from the cathode can be obtained from several promising highly effective electron emitters such as FEA and carbon nanotubes (CNT). Usually, to apply such a modulated electron beam to conventional microwave tubes, the required acceleration voltage V_b is so much larger than the modulation voltage V_{hf} that the initial beam configuration can be considered as a density modulated electron beam, $J=\rho u_0$, where

$$\rho=\rho_\lambda(z)\exp[-j(\omega t-\beta_e z)],\quad \beta_e=\frac{\omega}{u_0},$$

$$\rho_\lambda(z)=\sum_{m=-\infty}^{\infty}\rho_m\exp[-jm\beta_e z], \tag{13}$$

$$\text{where}\quad \rho_m=\frac{1}{\lambda}\int_0^\lambda \rho_\lambda(z)\exp[jm\beta_e z]dz.$$

Therefore, the initial current density configuration can be expanded into the sum of time harmonics[26,27]

$$J=\sum_{m=-\infty}^{\infty}\rho_m u_0\exp[-j(\omega t-\beta_e z-jm\beta_e z)]$$

$$=\sum_{m=-\infty}^{\infty}J_m\exp[-jm\omega t],$$

$$\text{where}\quad J_m=\rho_m u_0=\frac{u_0}{\lambda}\int_0^\lambda \rho_\lambda(z(t))u_0\exp[jm\beta_e z(t)]\times\left(\frac{dz}{u_0}\right)$$

$$=\frac{1}{T}\int_0^T J_T(t)\exp[jm\omega t]dt. \tag{14}$$

The magnitude (J_m) of each time harmonic is determined from the initial current density pattern, which is governed by a Fowler–Nordheim equation in practical form (1), where $V(t)=V_b(1+\varepsilon\sin\omega t)$, and ε is defined as a modulation depth; $\varepsilon=V_{\mathrm{hf}}/V_b$.

Equation (1) is a nonlinear equation, and the results can be obtained by numerical analysis. Figure 10 shows the results, where the bias voltage V_b is assumed to change depending on modulation depth to keep the average current I_{av} at the same level during one rf period. The emission pattern

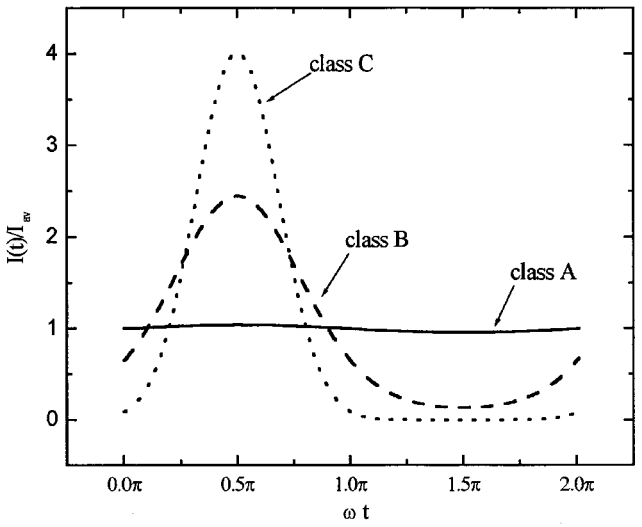

FIG. 10. Current density profile with respect to operation classes.

is classified by conduction angle: Class A operation (conduction angle=360°), class B operation (180°<conduction angle<360°), and class C operation (conduction angle <180°).[29] As the modulation depth increases, the operation class transits from A to C, and the normalized current $I(t)/I_{\mathrm{av}}$ profile becomes nonsinusoidal, where the higher harmonic components increase depending on Eq. (14). In this simulation, F–N coefficients (a, b) suggested by Jensen ($a=3.828[A/V^2]$, $b=345.2[V]$)[28] are used, where class A operation is obtained below the modulation depth $\varepsilon\sim10^{-2}$.

Figure 11 represents the simulation results of MAGIC[30] and a one-dimensional nonlinear code which is similar to that used in conventional TWT theory[10] (see also Ref. 31 for details). The slope of the output power versus modulation depth at fixed circuit length (50 mm), the so-called AM–AM conversion, shows a good linearity of output power with a moderate modulation depth (10^{-3}–10^{-2}). This means, contrary to the klystrode case in Sec. III, the tighter bunch from stronger modulation (class B, C operation) does not guaran-

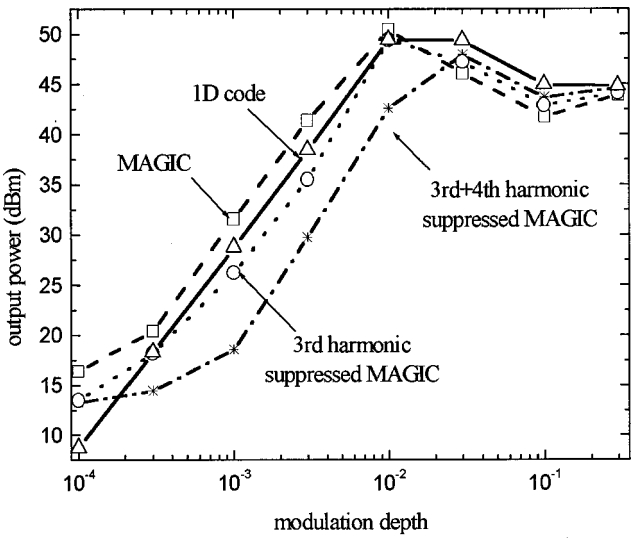

FIG. 11. Output power of twystrode at the saturated position.

tee a good performance due to the occurrence of higher harmonic components (Fig. 10). Rather, class A operation (with modulation depth between 10^{-3} and 10^{-2}) enables us to reach to sufficient output power level and linearity even without any tapering, which is mentioned in Ref. 9. Because higher harmonics are naturally considered in MAGIC simulations, in contrast to 1D nonlinear theory, we reduced the third or fourth harmonic in MAGIC simulations using attenuators with resonant loss[30] at each harmonic frequency to see the effects of higher harmonic components in the interaction. After the third or fourth harmonic is reduced, the output power simulated by MAGIC code increased to be closer to that of the 1D nonlinear code simulation at strong modulation regions. Here the poorer performance at class B and C operation can be attributed to higher harmonic components from the strongly modulated electron beam.

VII. CONCLUSION

In this paper a theoretical consideration of a number of microwave amplifiers and oscillators with FEAs is presented. The results demonstrate the potential advantages of microelectronic modifications of ''classic'' vacuum microwave devices. Using FEAs in such devices as traveling wave klystrons, klystrodes and twystrodes gives an opportunity to achieve performance superior to devices with thermionic cathodes. Microelectronic cross-field amplifiers seem to be very promising devices, since they do not require a controlling grid and electron beam focusing and allow one to use disordered emitting surfaces, such as diamond-like carbon films and carbon nanotubes, instead of uniform regular arrays. We also emphasize the advantage of the vacuum microtriode oscillator as a new source of chaotic microwave radiation. The combination of ideas and methods of nonlinear dynamics with modern vacuum microelectronic technologies may be useful for practical applications in communication and information processing systems.

ACKNOWLEDGMENTS

This work is partly supported by the USA Civilian Research and Development Foundation (Award No REC-006) and partly by the Ministry of Science and Technology of the Republic of Korea through the National Research Laboratory Program.

[1] I. Brodie and C. A. Spindt, Adv. Electron. Electron Phys. **83**, 106 (1992).
[2] V. A. Isayev, D. V. Sokolov, and D. I. Trubetskov, Radiotekh. Elektron. (Moscow) **35**, 2241 (1990); [Sov. J. Commun. Technol. Electron. **36**, 64 (1991)].
[3] I. Brodie and P. R. Schwoebel, Proc. IEEE **82**, 1006 (1994).
[4] D. I. Trubetskov, A. G. Rozhnev, and D. V. Sokolov, *Lectures on Micro-Wave Vacuum Microelectronics* (College Press, Saratov, 1996) [in Russian].
[5] Special issue on noncoherent chaotic communications, IEEE Trans. Circuits Syst. Part 1 **47**, 1661 (2000).
[6] J. P. Calame, H. F. Gray, and J. L. Shaw, J. Appl. Phys. **73**, 1485 (1993).
[7] M. A. Kodis, K. L. Jensen, E. G. Zaidman, B. Goplen, and D. N. Smith, IEEE Trans. Plasma Sci. **24**, 970 (1996).
[8] F. Charbonnier, J. Vac. Sci. Technol. B **16**, 880 (1998).
[9] D. R. Whaley, B. M. Gannon, C. R. Smith, C. A. Armstrong, and C. A. Spindt, IEEE Trans. Plasma Sci. **28**, 727 (2000).
[10] J. Rowe, *Nonlinear Electron Wave Interaction Phenomena* (Academic, New York, 1965).
[11] W. J. Pohl, IEEE Trans. Electron Devices **12**, 361 (1965).
[12] D. H. Priest and M. B. Shrader, Proc. IEEE **70**, 1318 (1982).
[13] D. H. Priest and M. B. Shrader, IEEE Trans. Electron Devices **38**, 2205 (1991).
[14] K. Nyguen, G. D. Warren, L. Ludeking, and B. Goplen, IEEE Trans. Electron Devices **38**, 2212 (1991).
[15] F. M. Charbonnier, J. P. Barbour, L. F. Garrett, and W. P. Dyke, Proc. IEEE **51**, 991 (1963).
[16] N. M. Ryskin, Electron. Lett. **32**, 195 (1996).
[17] N. M. Ryskin, *Tech. Digest, 9th International Vacuum Microelectronics Conference*, St. Petersburg, Russia, 1996, edited by Yu. V. Gulyaev, (Nevskyi Courier Publ., St. Petersburg, 1996), p. 606.
[18] N. M. Ryskin, Radiophys. Quantum Electron. **40**, 1511 (1997).
[19] C. A. Spindt, I. Brodie, L. Humphrey, and E. R. Westerberg, J. Appl. Phys. **47**, 5248 (1976).
[20] D. V. Sokolov and D. I. Trubetskov, *Tech. Digest, 9th International Vacuum Microelectronics Conference*, St. Petersburg, Russia, 1996, edited by Yu. V. Gulyaev (Nevskyi Courier Publ., St. Petersburg, 1996), p. 601.
[21] D. V. Sokolov and D. I. Trubetskov, Zh. Tekh. Fiz. **70** 136 (2000) [Tech. Phys. **45**, 134 (2000)].
[22] *Crossed-field Microwave Devices*, edited by E. Okress (Academic, New York, London, 1961).
[23] N. I. Sinitsyn, Yu. V. Gulyaev, M. B. Golant, I. S. Nefedov, G. V. Torgashov, Yu. F. Zakharchenko, and A. I. Zhbanov, J. Vac. Sci. Technol. B **11**, 477 (1993).
[24] D. I. Trubetskov, E. S. Mchedlova, V. G. Anfinogentov, V. I. Ponomarenko, and N. M. Ryskin, Chaos **6**, 358 (1996).
[25] V. I. Ponomarenko and D. I. Trubetskov, Dokl. Phys. **39**, 562 (1994).
[26] H. G. Kosmahl, IEEE Trans. Electron Devices **36**, 2728 (1989).
[27] E. G. Zaidman and M. A. Kodis, IEEE Trans. Electron Devices **36**, 2728 (1989).
[28] K. L. Jensen, J. Appl. Phys. **83**, 7982 (1998).
[29] J. C. Whitaker, *Power Vacuum Tubes Handbook* (Van Nostrand Reinhold, New York, 1994), p. 46.
[30] L. Ludeking, D. Smithe, M. Bettenhausen, and S. Hayes, MAGIC *User's Manual* (MRC/WDC-R-445, 1999).
[31] S. S. Jung, A. V. Soukov, and G. S. Park, J. Korean Phys. Soc. **39**, 1087 (2001).